Surface & Coatings Technology 364 (2019) 239–247

Contents lists available at ScienceDirect

Surface & Coatings Technology

journal homepage: www.elsevier.com/locate/surfcoat

Development of an in-situ chitosan-copper nanoparticle coating by electrophoretic deposition

E. Tabesh[a], H.R. Salimijazi[a,*], M. Kharaziha[a], M. Mahmoudi[a], M. Hejazi[b]

[a] Department of Materials Engineering, Isfahan University of Technology, Isfahan 84156-83111, Iran
[b] Department of Textile Engineering, Isfahan University of Technology, Isfahan 84156-83111, Iran

ARTICLE INFO

Keywords:
Chitosan
Copper nanoparticle
Electrophoretic deposition
Antibacterial
Corrosion resistance

ABSTRACT

The aim of this study was to develop a chitosan-copper nanocomposite coating on stainless steel 316L to improve the antibacterial properties and corrosion resistance of the substrate. After in-situ synthesizing of chitosan-modified Cu nanoparticles, electrophoretic deposition was utilized to deposit chitosan-copper nanocomposite coatings consisting of various amounts of Cu nanoparticles. Moreover, the role of various deposition parameters such as time and voltage on the coating properties was investigated. Physical and chemical properties of the synthesized Cu nanoparticles and the nanocomposite coatings were analyzed using X-ray diffraction (XRD), scanning electron microscopy (SEM), coupled with the Energy-Dispersive Spectroscopy (EDS), Fourier transform infrared spectroscopy (FTIR) and transmission electron microscopy (TEM). The corrosion resistance of coatings was measured by electrochemical measurements such as tafel and electrochemical impedance spectroscopy (EIS) tests. The antibacterial properties of nanocomposite coatings were analyzed using several Gram-positive and Gram-negative microorganisms, including methicillin-resistant *Staphylococcus aureus* and *Escherichia coli*. Results confirmed that Cu nanoparticles were synthesized with an average size of 11 ± 6 nm. Moreover, the incorporation of 0.5 wt% copper nanoparticle in the chitosan coating under 20 V and 5 min conditions resulted in the formation of uniform and crack-free nanocomposite coating with a thickness of about 17 μm. Results confirmed a significant improvement in the antibacterial activity and corrosion resistance of 316L stainless steel substrates. In conclusion, chitosan-copper nanocomposites could be considered as a good candidate for increasing the antibacterial properties and corrosion resistance to prevent infections in biomaterials applications.

1. Introduction

The quality of human life has been promoted by restoring the mobility and function of injured organs by using implants as supporters or substitutions. Despite significant progress and advantages, the major clinical challenges are implant-associated infections leading to implant failure and chronic diseases [1,2]. In addition to implant-associated infections, corrosion sensitivity is another challenge treating the metallic implants. Among various types of metallic biomaterials, thanks to its acceptable mechanical properties, stainless steel has been widely applied for various kinds of orthopedic implants. However, some clinical investigations have reported that these alloys undergo implant-associated infections and severe corrosion under physiological conditions [1,3–5]. Thus, finding a method for increasing the performance of these alloys is very important.

In recent years, there have been growing interest in corrosion resistant and/or antibacterial coatings namely nanohydroxyapatite, TiO_2, and chitosan on metallic alloys [6–9]. However, most of them were used as a mono-protective layer. Although the studies on the organic/inorganic composite coatings on metallic implants, especially stainless steel, were limited, some special surface advancement of nanocomposite coatings increased the corrosion resistance and antibacterial activity of coatings at the same time [10]. Various types of antibacterial polymers (e.g. poly(3-hydroxybutyrate-*co*-3-hydroxyvalerate) (PHBV) [11]) have been used as coatings for biomedical applications. Among them, chitosan-based coatings with strong antibacterial and corrosion resistant properties have been proposed as a promising strategy to destroy bacteria and decrease corrosion of substrate [1,4,5]. For example, Pang et al. [12] showed the ability of EPD method in order to fabricate the composite coating containing Hydroxyapatite, $CaSiO_3$, and chitosan which provided corrosion protection of the stainless steel substrate [12]. In other research, they investigated the corrosion resistance of Hydroxyapatite-Chitosan composite coating and showed that this coating provided the corrosion protection of the 316L stainless steel

* Corresponding author.
E-mail address: hrjazi@cc.iut.ac.ir (H.R. Salimijazi).

https://doi.org/10.1016/j.surfcoat.2019.02.040
Received 17 November 2018; Received in revised form 21 January 2019; Accepted 13 February 2019
Available online 22 February 2019

substrate [13]. In order to thrive the antibacterial activity against both types of bacteria, various types of antibacterial agents such as metal nanoparticle (Cu [14,15], Ag [16,17]) have been combined with chitosan to develop antibacterial nanocomposite materials. Among them, copper nanoparticles have been attracted for biomedical applications. For instance, Wen-Li et al. [18] showed that the antibacterial activity of chitosan/metal complexes was remarkably improved compared to the pure polymer and metal nanoparticles (Cu^{2+} and Zn^{2+}) [18].

Accordingly, various techniques have been applied to develop nanocomposite coatings based on chitosan, consisting of sol-gel [19], layer by layer [20] and electrophoretic deposition technique [21]. Among them, the electrophoretic deposition (EPD) approach has been introduced as a rapid, easy process, cost-effective, site-selective, and multi-functional technique. EPD can produce a uniform and stable coatings with tunable thickness at room temperature [22–24]. This technique has been widely applied to develop various ceramic, polymeric and nanocomposite coating for various applications [22,24,25]. Furthermore, agglomeration of nanoparticles is another issue which is common during the preparation of the coating process. In this respect, in-situ synthesizing of nanocomposite and coating could be an alternative to overcome agglomeration of nanoparticles.

The aim of this study was to develop chitosan-copper nanoparticle coating on stainless steel in order to simultaneously improve antibacterial property and corrosion resistance. In this regard, after synthesizing chitosan-modified copper nanoparticles, nanocomposite coatings consisting of various amounts of Cu nanoparticles were developed using the EPD process. Moreover, physical and chemical properties, antibacterial activity and the corrosion stability of the coatings in the simulated body fluid (SBF) were investigated.

2. Materials and methods

2.1. Materials

Copper sulfate pentahydrate ($CuSO_4{\cdot}5H_2O$), chitosan (powder, medium molecular weight), acetic acid (CH_3CO_2H), sodium hydroxide (NaOH), ascorbic acid ($C_6H_8O_6$), hydrazine hydrate (NH_2NH_2) and ethanol (C_2H_5OH) were supplied by Merck, Germany.

2.2. Sample preparation

AISI 316L samples were used as the substrates with a dimension of $20 \times 10 \times 1\ mm^3$. Firstly, the samples were polished using SiC papers with the grit sizes of 600. Consequently, AISI 316L substrates were cleaned ultrasonically in acetone and then in deionized water for 30 min, in order to remove residual greases and surface impurities.

2.3. Synthesis of chitosan-modified copper nanoparticles

Chitosan-modified copper nanoparticles were synthesized by using the chemical process. Two primarily solutions, the first one consisting of copper precursor (0.05 M $CuSO_4.5H_2O$ aqueous solution) and the second one consisting of chitosan (0.4 wt% chitosan in 0.1 M acetic acid) were separately prepared and mixed. After 30 min of mixing these two solutions with a volume ratio of 1:4 (copper precursor solution: chitosan solution in 100 ml solution), the color of the solution changed to blue. Following, to prevent the oxidation of copper nanoparticles, 1 ml of 0.05 M ascorbic acid was dropwisely added to the solution. Then, after the addition of 4 ml of 0.6 M NaOH, the pH of the solution was adjusted to 4 leading to change in the color of the solution to green. Finally, hydrazine hydrate (1 ml), as a reduction agent, was added to the solution to obtain a dark brown color indicating the formation of copper nanoparticles. During all steps of the process, the temperature of the solution was kept constant at 60 °C, while the solution was stirred magnetically.

2.4. Fabrication of chitosan-copper nanoparticle coatings

Chitosan-copper nanoparticle coatings were developed using the EPD process. In the first stage of the solution preparation process for coating, the copper nanoparticles were synthesized in a solution including chitosan and acetic acid as stabilizer and modifier. Then, the solution was centrifuged and dried overnight to obtain copper nanoparticles. The prepared copper nanoparticles were slightly added to the coating solution containing (1 vol% acetic acid, 1 wt% chitosan in a ratio of water:ethanol of 20:80). However, there was a significant aggregation of nanoparticles leading to the formation of an inappropriate coating on the substrate and the deposited coating had a high amount of agglomerated particles. To solve this problem, various amount of copper precursor were incorporated in the coating solution to initially produce copper nanoparticles followed by in-situ deposition of coating with different copper concentration (0.25, 0.5, 1 and 1.25 wt%). Prior to the coating deposition, the solution was sonicated for 30 min to obtain a homogenous solution. The constant voltage was applied by using a power supply (SL20200J IPC). The EPD process was carried out at a constant cathode and anode distance of 10 mm under various times (1, 5, 10, and 15 min) and voltages (5, 10, 20, 30 and 40 V) conditions to optimize the properties of the coatings.

2.5. Characterization of the chitosan-copper nanoparticle coatings

Phase composition of the synthesized powders was characterized by X-ray diffraction (XRD, Philips) with monochromatized Cu-Kα radiation (40 kV, 80 mA)). In order to determine the functional groups of chitosan and synthesized copper nanoparticles, Fourier Transform Infrared (FTIR) spectroscopy was performed by Bruker Tensor-27 in the range of 600–4000 cm^{-1}. Transmission Electron Microscope (TEM, Philips EM208S 100 kV Netherland) was used to evaluate the morphology and size of Cu nanoparticles. Moreover, the particle size of powders was measured using Image J software ($n = 80$). Furthermore, Scanning Electron Microscope (SEM, Philips XL30) was utilized to evaluate the distribution of copper nanoparticles within the coatings and also to measure the thickness of the coatings. In addition, Energy-Dispersive Spectroscopy (EDS) analysis was used to determine the composition of the coatings. Furthermore, scratch tests were carried out in order to measure interfacial adhesion strength between the nanocomposite coatings and substrate based on ASTM D7027-13. In this test, a diamond-stylus scratch tester (tip radius and scratch length respectively were 22 μm and 1 mm) was performed on the coatings with a linearly increasing load in the range of 30–90 N under a constant speed of 10 mm/min followed by reaching a load in which coating was failed. Consequently, the first load force in which the coating exhibited a failure was reported as the critical load to determine the adhesion strength of the coatings [26].

2.6. Electrochemical tests

Electrochemical measurements such as open circuit potential (OCP) with time, electrochemical impedance spectrophotometry (EIS) and Tafel polarization test were carried out in a simulated body fluid (SBF) at pH = 7.4. The SBF was made according to Kokubo et al. [27] protocol. The corrosion tests were performed at room temperature (around 25 °C) using the IVIUMSTAT potentiostat corrosion measuring system. A three-electrode system, i.e. a sample as a working electrode, a platinum sheet as a counter electrode, and a KCl saturated calomel electrode (SCE) as a reference electrode were used. OCP changes with time were recorded for up to 30 min of immersion in the solution. Subsequently, the EIS analysis was performed at a frequency of 10 kHz to 10 mHz using a 10 mV sinusoidal signal at OCP. Then, Tafel polarization test was used by scanning potential of −0.25 V_{SCE} vs. OCP to +1.00 V_{SCE} vs. OCP at a potential scan rate of 1 mV/s. In order to analyze the data from the Tafel polarization plots and to simulate the data obtained

from EIS curves, various electrochemical parameters of the graphs were extracted using CorrView and Ivium software, respectively. ZView software was used to fit the EIS data.

2.7. Antibacterial activity test

In order to evaluate the antimicrobial activity of the nanocomposite coatings, firstly gram-positive and gram-negative bacteria such as *S. aureus* and *E. coli* were cultured in a 10 ml nutrient broth consisted of 3.0 g/l beef extract, 5.0 g/l peptone and 1000 ml of distilled water at pH 6.8 ± 0.2, simultaneously. Nanocomposite coated samples with a dimension of 2 × 2 cm^2 were sterilized, based on ASTM E2149. In following, each sample separately was placed in a sterile petri dish and 100 µl of medium culture included either *Escherichia coli* (*K*-12) or *Staphylococcus aureus* (ATCC 12600) at 10^4–10^5 CFU/ml was added onto their surface. After 1 h incubation at 37 °C and 5% CO_2, samples were placed into 10 ml of sterile water, followed by strenuously shaking for 5 min. Then prior to incubating for 24 h at 37 °C and 5% CO_2, each sample was diluted in an agar plate. Eventually, a light microscope was used to count colonies formed on each sample by quantization of the colony forming units (CFU).

2.8. Statistical analysis

The data were reported as mean ± standard deviation (SD) and one-way ANOVA analysis was used in order to measure the statistical significance followed by Tukey's multiple comparisons using GraphPad, Prism Software (V.5). Differences were taken to be significant for $P < 0.05$.

3. Results and discussions

3.1. Characterization of chitosan-modified copper nanoparticle

At first, chitosan modified copper nanoparticles were synthesized in the chitosan-based solution. XRD pattern of the synthesized copper nanoparticle (Fig. 1 a) revealed the formation of pure copper phase. The characteristic peaks appeared at 2θ = 43.3°, 50.4°, 74.1°, 89.9°, and 95.1° were related to plane index of (111), (200), (220), (311), and (222) of copper with face centered cubic structure, respectively, according to standard card (00–001-1241 (ICSD code)). However, the small peak could be detected at around 2θ = 20° assigned to the characteristic peak of chitosan confirming that chitosan covered the nanoparticles to avoid agglomeration during the synthesis process. This behavior might affect the antimicrobial property of Cu-based components [28]. The mechanism of chitosan (Cts) encapsulating copper nanoparticles produced through chemical reduction is shown schematically in the inset image in Fig. 1 a and the chemical reaction is showed in Eq. (1) [28]:

$$2[Cu(Cts)]^{+aq} + N_2H_4 \rightarrow 2[Cu(Cts)] + N_2 + 2H_2O \quad (1)$$

Moreover, no peak was assigned to the CuO or Cu_2O phases, which is known as the most common impurity in the synthesis process of copper. It might be due to the role of chitosan to protect Cu nanoparticles against the synthesis process from Cu to CuO or Cu_2O transformation. This behavior was similarly reported in previous researches [14,15]. For instance, Usman et al. [29] showed that increasing the chitosan concentration resulted in enhanced purity and reduced particle size of Cu nanoparticles.

The interaction between chitosan and copper nanoparticles was evaluated via FTIR spectroscopy (Fig. 1 b). FTIR spectrum of chitosan consisted of a peak at 3358 cm^{-1} ascribed to overlap N—H and O—H stretching bonds. The absorption bands located at 2878 cm^{-1} and 1658 cm^{-1} were related to C—H stretching and the bonds at 1606 cm^{-1} were attributed to N—H bending. Furthermore, the absorption bands located at 1358 cm^{-1}, 1318 cm^{-1} and 1028 cm^{-1} were corresponded to C—H bending and C—O stretching bonds, respectively. After formation of chitosan-copper interfaces, the intensity of some of these bands reduced and some of them shifted confirming the interaction between chitosan and copper. For instance, N—H stretching bonds moved from 1606 cm^{-1} to 1601 cm^{-1} and the peaks located at 1658 cm^{-1} and at the range of 1318–1429 cm^{-1} were completely removed which might be related to covering the copper nanoparticles by N—H groups of chitosan [23,30]. In addition, new peaks appeared at approximately 629 cm^{-1}, which could be assigned to an interaction between chitosan and copper nanoparticles, were related to Cu—N stretching vibrations and Cu—O bonds [31].

Fig. 2 shows TEM images and histogram chart of synthesized copper nanoparticles. TEM image (Fig. 2 a) indicated that Cu nanoparticles with spherical morphology and without any significant agglomeration were synthesized. Moreover, the particles size distribution of Cu nanoparticle (Fig. 2 b) revealed the formation of uniform particles with an average size of 11 ± 6 nm. This result was in a good agreement with Usman et al. [28] and Dang et al. [32] indicating the effects of chitosan concentration on the uniformity of copper nanoparticles.

3.2. Characterization of chitosan-copper nanoparticle coatings

Electrophoretic deposition was carried out at various times (1, 5, 10, and 15 min) and voltages (5, 10, 20, 30 and 40 V). According to Fig. 3, the thickness of the EPD coatings was enhanced over increasing the voltage and the time of the electrophoretic process [24]. Although there was a significant increase in the thickness of the coating at a higher voltage at a constant time (5 min) (Fig. 3 a), the coating was separated from the substrate in 40 V (cross-section images are presented in Fig. 3 a). In addition, at a constant voltage of 20 V, the thickness of the coating was slightly enhanced upon increasing the time of EPD time. Thus, the effect of voltage on the thickness of the coating was higher than time due to the improvement of the mobility and proper

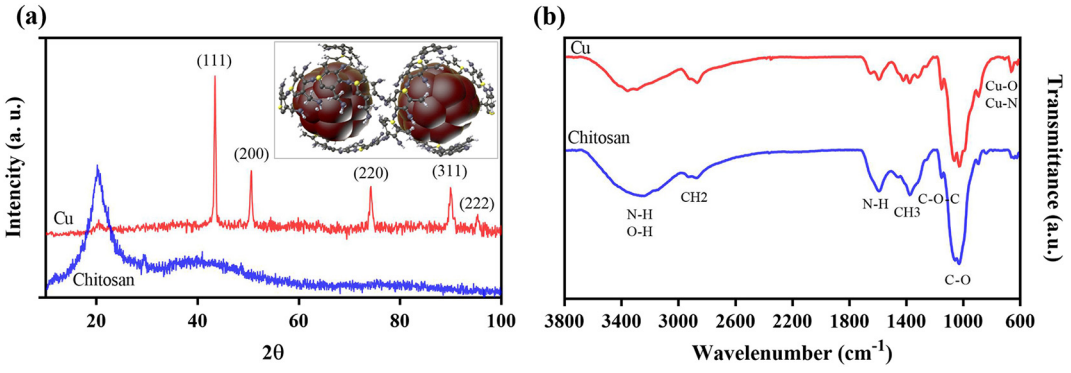

Fig. 1. a) XRD pattern and b) FTIR spectra of chitosan and copper nanoparticles. Inset in section a: Core-shell structure of copper nanoparticle in chitosan.

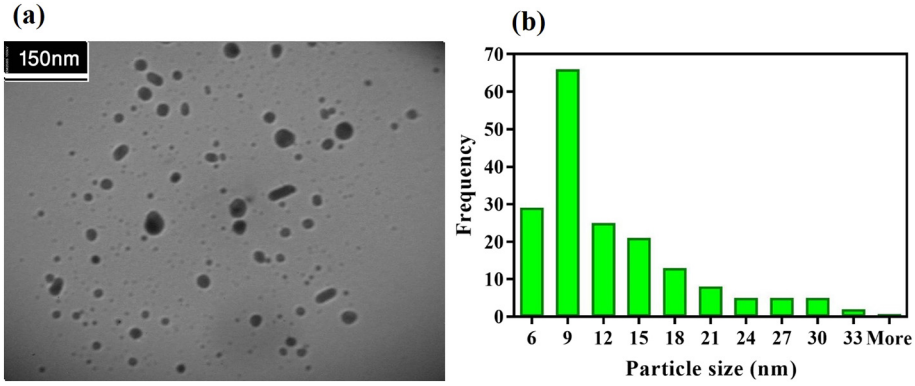

Fig. 2. a) TEM image and b) frequency histogram of particle size of copper nanoparticles.

orientation of chitosan. In fact, voltage navigated chitosan to settle on the coating. In accordance to the literature, Zhitomirsky et al. [33] showed that the thickness of the coating, which is developed using EPD process, was affected by different parameters such as time and voltage of the process, as below (Eq. (2)):

$$\rho Ax = \frac{C\mu Ut}{d} \tag{2}$$

where ρ is the apparent density, A is the surface area of the electrode, x is the thickness of the coating, C is the concentration of the particles in the suspension, μ is the mobility of the particles, U is the applied voltage of EPD, t is the time of the process, and d is the distance between the two electrodes. According to Eq. (2), a higher thickness of coating could be achieved by increasing the voltage. The applied force on particles, which was increased in higher voltages, increased the possibility of moving these agglomerated particles in the suspension. Thus, the particles might have less time to lie in suitable locations which weaken the adhesion strength of coatings and corrosion resistance [33].

Fig. 4 a and b show the critical load force (as a measurement of the adhesion strength of the coatings) as a function of the voltage and time. According to Fig. 4 a, an upward trend could be detected in the value of critical load (deformation force) when the voltage of the EPD process increased. However, there was a peak in the force value at 85 gf (0.85 N) for coatings deposited under 20 V and 30 V. The bonding adhesion of the coatings decreased at higher voltages followed by decreasing packing density of the coating. It could be due to the formation of water bubbles during the EPD process (inset image in Fig. 5 a shows the light microscopy image of the sample prepared at 40 V). Thus, there should be an optimum voltage of 20 V and 30 V for this deposition process. Fig. 4 b shows the effect of time of the EPD process on the loading force. The bonding adhesion of the coatings increases at a higher time of EPD process from 1 min to 5 min. Subsequently, the adhesion of the coating remained constant as EPD time went up. It is concluded that the most uniform coating, with regards to the surface morphology, thickness, adhesion, and absence of bubbles underneath of the coating, is reached under 20 V for 5 min [1].

In the light of the cationic nature and good properties of film forming of chitosan, it can be coated independently to create coatings of pure polymer [34]. Chitosan also provides effective electrosteric stabilization of metal particles. In addition, Chitosan could be adsorbed on the surface of Cu nanoparticles and provides a positive charge which allows cathodic electrodeposition of particles [35]. Furthermore, chitosan, as an efficient binder, prevents cracking and provides adhesion of the coating to the substrate [21,35]. It had been proven that the usage

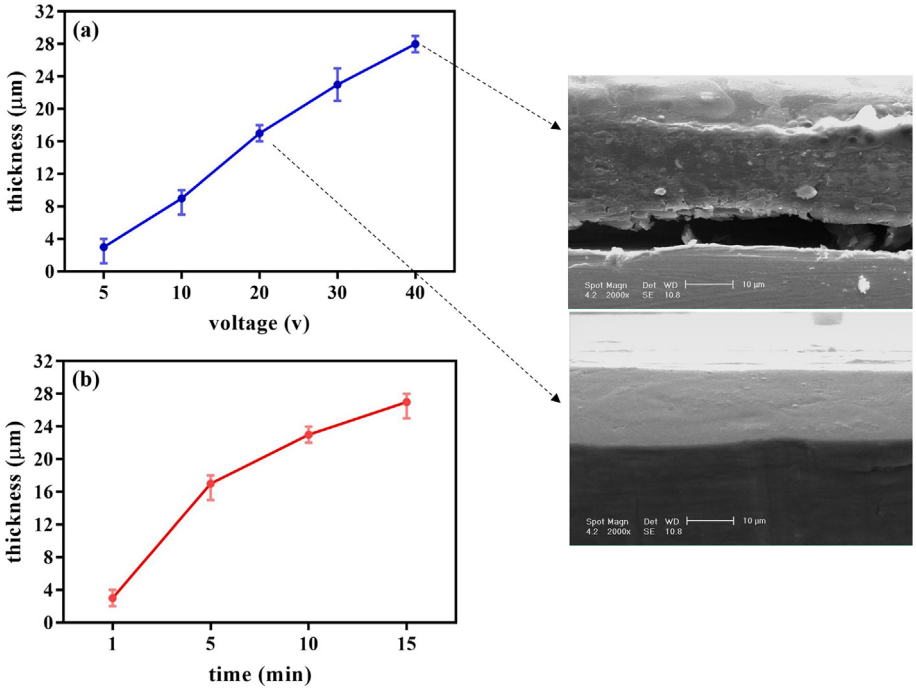

Fig. 3. Effect of a) voltage at 5 min and b) time at 20 V on the thickness of the coating.

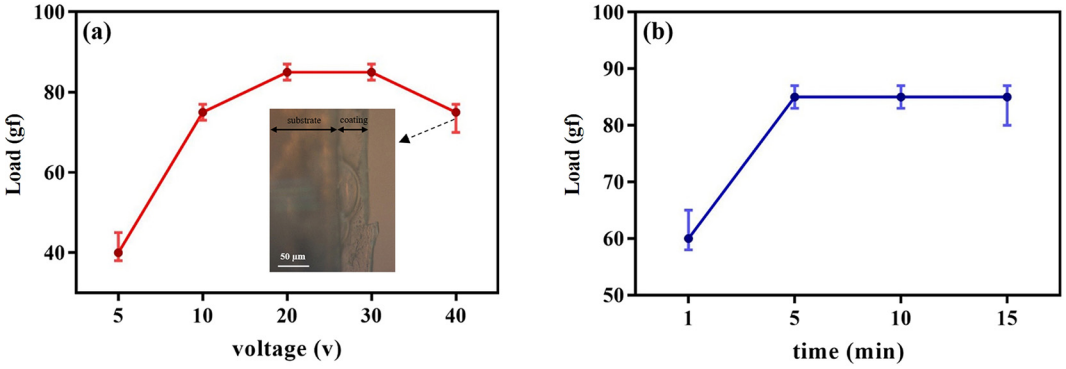

Fig. 4. Effect of a) voltage at 5 min, b) time at 20 V and on deformation force of coating.

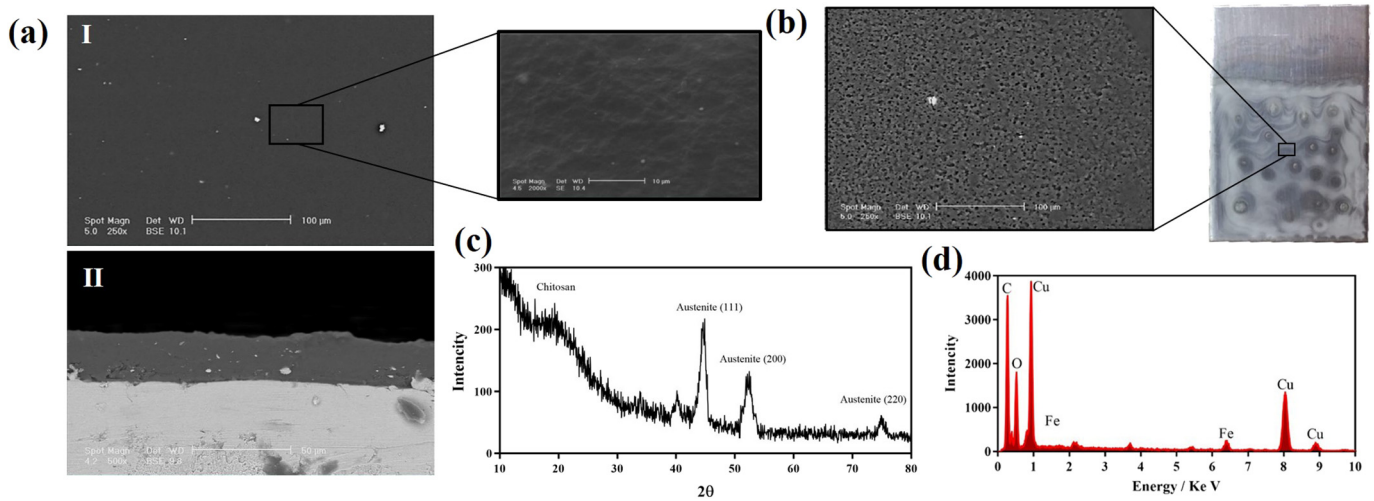

Fig. 5. Scanning electron microscope (SEM) image of coating at 20 V and 5 min: a) 0.5% (I: surface and II: cross-section of the coating), b) 1.25% Copper nanoparticles and c) EDS spectrum of nanocomposite coating.

of chitosan can enable the formation of cathodic electrophoretic deposition of coating with various materials and interfacial bonding of the particles.

In order to improve the previous researches, we utilized the chitosan suspension with various Cu contents to deposit chitosan-copper coatings [35]. Our results indicated that EPD could enable the formation of chitosan-copper nanocomposite coating.

Fig. 5. a and b show the SEM images of the nanocomposite coatings, consisting of two different concentration of Cu nanoparticles, deposited at optimum process parameters (at 20 V and 5 min). In the lower Cu nanoparticle content (0.5 wt%), the copper nanoparticles were uniformly distributed throughout the chitosan-based coating. Inset image in Fig. 5 a.I indicates the smooth continuous morphology of coating in the presence of Cu nanoparticles at higher magnification. Due to the fact that heavier atoms such as copper are brighter than chitosan, the BSE image (Fig. 5 a) proved that these light points were related to the Cu atoms in the coating. The cross-section image of the coating consisting of 0.5% Cu nanoparticles (Fig. 5 a.II) demonstrated the almost uniform distribution of Cu nanoparticles in the chitosan-based matrix. Fig. 5 c shows the grazing XRD pattern of the nanocomposite coating. The characteristic peaks appeared at $2\theta = 44^\circ$, 54° and 75° were related to the plane index of (111), (200), and (220) of stainless steel 316L, respectively. In addition, the small peak at around $2\theta = 20^\circ$ assigned to the characteristic peak of chitosan. Due to the low concentration of the Cu nanoparticles in the coating, there was no peak related to Cu nanoparticles. In order to investigate the presence of Cu nanoparticles in the coating, the EDS analysis was used. EDS analysis (Fig. 5 d) also confirmed the presence of Cu atoms accompanied by Fe signals related to the stainless-steel substrate. Moreover, C and O signals belonged to chitosan that was previously recognized by XRD analysis.

SEM images of coatings in Fig. 5 showed that the microstructure of the nanocomposite coating strongly relied on the composition of the coating. In a high concentration of copper (i.e. > 1%), nanoparticles emerged onto the surface of the coating (Fig. 5 b). Conversely, in a low concentration of copper nanoparticles (i.e. < 1%), they were well-embedded in the chitosan matrix and the coating remained smooth and crack-free, which could be due to the steady electrophoretic mobility of polymer during deposition. In fact, due to different electrophoretic deposition mechanisms and deposition rates of Cu nanoparticles and chitosan, it was suggested that the presence of lower content of Cu nanoparticles led to avoid massive deposition and agglomeration of Cu nanoparticle upon DEP in order to obtain a uniform coating. Similar statements were reported by other research for organic-inorganic composites [24].

3.3. Corrosion resistance evaluation of the nanocomposite coatings

Fig. 6 shows the OCPs of the uncoated, chitosan coated, and chitosan-copper nanocomposite coated samples. All specimens reached to the stability after about 1200 s of immersion in the SBF solution (pH = 7.4) at room temperature (about 25 °C). The OCP value of the uncoated sample moved to negative values after immersion. While the OCP values of all coated samples moved to positive values after immersion, and became ennobled, which probably was due to the chitosan formation on the surface of stainless steel. During the immersion period of 1800 s, the OCP values of all chitosan-copper nanocomposite coated

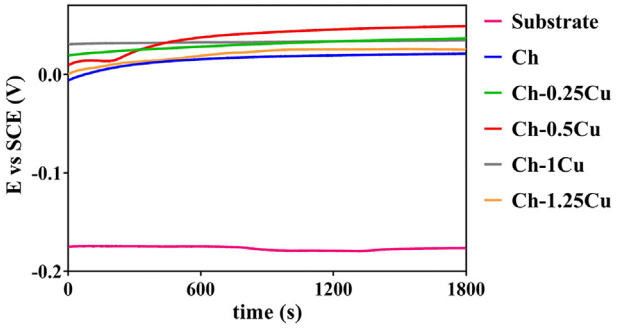

Fig. 6. OCPs of the blank substrate and chitosan coating alone and chitosan-copper nanocomposite coating samples immersed in SBF solution (pH = 7.4) at room temperature.

samples were higher than those of the uncoated and chitosan coated samples. By increasing the Cu concentration of coating from 0.25 to 1.25 wt%, firstly, the OCP values increased and then, reduced. Thus, the Ch-0.5Cu sample had the highest OCP value in all samples during the immersion time, which could be due to its higher compaction and uniformity of coating, and it was stable at about 0.05 V_{SCE}.

Fig. 7 illustrates the experimental and simulated Nyquist graphs of the samples after immersion in the SBF at room temperature. The spectra were as well defined as in the impedance spectrum for all specimens at high-frequencies to low-frequencies. The obtained Nyquist graphs were similar to the previously reported results for a natural polymeric coating consisting of chitosan and gold nanoparticles electrodeposited on NiTi alloy [36]. The impedance of the chitosan coated sample in our study was higher than that of the uncoated one, which was similar to the chitosan coating on the NiTi alloy [36]. This clearly confirmed the effect of chitosan layer on increasing the corrosion resistance of stainless steel. Furthermore, by an increase in the Cu concentration up to 0.5 wt%, impedance enhanced due to higher compaction and uniformity of coating, which caused a reduction of the penetration rate of the solution into the coating. By increasing the Cu concentration of coating to higher values than 0.5%, the impedance decreased due to the agglomeration of Cu nanoparticles and less bonding between the coating and substrate. Therefore, the impedance of the Ch-0.5Cu sample was the highest, which reflected the highest corrosion resistance of the Ch-0.5Cu sample.

The experimental data were fitted by using the electrical elements described in the circuits inserted in Fig. 7, which was similar to the reported results by other researches [36]. The circuits consisted of: R_s, the electrolyte resistance between the working and the reference electrodes, R_b and CPE_{ox}, the barrier resistance and the constant phase element of the native oxide layer of stainless steel, respectively. R_1, R_2 and CPE_1, CPE_2, are the electrical resistance and the constant phase

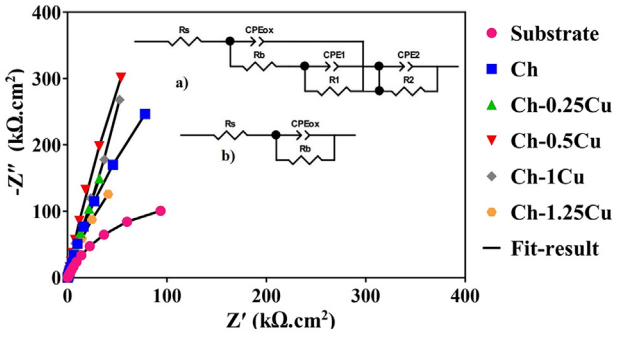

Fig. 7. the experimental and simulated Nyquist graphs of the samples after immersion in SBF (pH = 7.4) at room temperature along with the equivalent circuit used to simulate experimental impedance data a) chitosan coating and chitosan-copper nanocomposite coating samples and b) blank substrate.

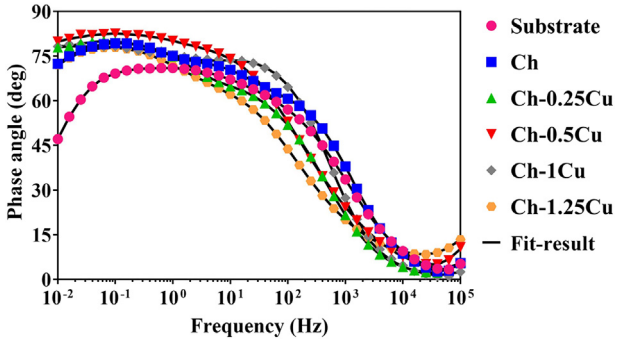

Fig. 8. Bode-phase graphs of the samples after immersion in SBF (pH = 7.4) at room temperature.

element of the chitosan and the chitosan-copper nanocomposite coatings, respectively. The electrical circuit was used to simulate the experimental data of chitosan and chitosan-copper nanocomposite coated samples consisting of three interfaces, one inner layer (native oxide layer of stainless steel) and one outer layer (chitosan and chitosan-copper nanocomposite coatings). Due to the surface roughness and heterogeneity in each interfaces, the constant phase element (CPE) was used instead of an ideal capacitor as well as n represented a deviation from ideal behavior. The impedance of the CPE was described in ref. [37].

According to Bode-phase graphs in Fig. 8, at high-frequencies, the phase angle of the uncoated sample was around 0°, which displayed that the impedance was dominated by electrolyte resistance. While, the phase angles of the coated samples were around 10°, indicating that the impedance was a capacitive response, which was related to the coating layer. Additionally, the phase angles of chitosan-copper nanocomposite coated samples were more than the phase angle of chitosan coated sample, which suggested that adding Cu nanoparticles to chitosan coating could improve the capacitive behavior of chitosan coating. At mid-frequencies, the phase angles of the uncoated and coated samples were related to a capacitive response of the native oxide layer of stainless steel that the phase angle changed due to change in the polar resistance of the oxide layer. Furthermore, the phase angles of chitosan coated samples (around 80°) were higher than that of the uncoated sample (around 70°), which showed that the coatings improved the native oxide layer of stainless steel. The result is in a good agreement with other researches on the electrophoretic deposition of chitosan on stainless steel [7,23,38]. By increasing the Cu concentration up to 0.5 wt%, the phase angle increased. But, in > 0.5 wt%, the phase angle reduced indicating that the Ch-0.5Cu sample was the lowest corrosion rate.

Fig. 9 shows the Bode-Z graphs of samples. At both high and low–frequencies, the impedance value of the Ch-0.5Cu sample was approximately the highest, which proved its higher corrosion resistance

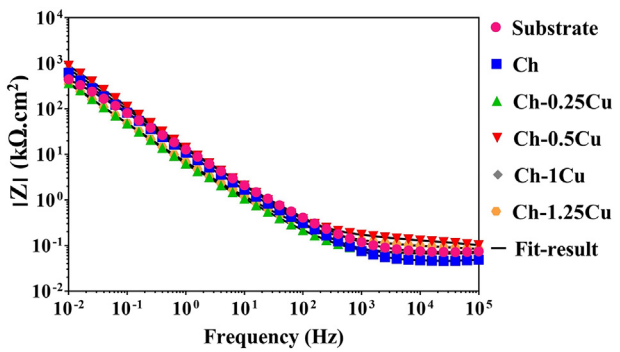

Fig. 9. Bode-Z graphs of the samples after immersion in SBF (pH = 7.4) at room temperature.

Table 1
Simulated parameters of EIS data of the samples using the proposed equivalent circuits.

Coating types	Inner layer			Outer layer					
	CPEox ($\mu F \cdot cm^{-2}$)	n	R_b ($\Omega \cdot cm^2$)	CPE_1 ($\mu F \cdot cm^{-2}$)	n	R_1 ($k\Omega \cdot cm^2$)	CPE_2 ($\mu F \cdot cm^{-2}$)	n	R_2 ($\Omega \cdot cm^2$)
Substrate	0.57	0.78	4.23	–	–	–	–	–	–
Ch	0.14	0.91	7.89	0.41	0.89	1.51	0.42	0.97	142.6
Ch-0.25Cu	0.11	0.84	16.98	0.75	0.77	2.30	0.71	0.79	178.4
Ch-0.5Cu	0.01	0.73	44.78	0.30	0.86	9.40	0.27	0.88	55.8
Ch-1Cu	0.06	0.79	18.09	0.42	0.94	4.60	0.96	0.94	565.7
Ch-1.25Cu	0.16	0.94	13.06	0.80	0.81	6.70	0.52	0.95	170.3

compared to the others. On the other hand, the impedance value of chitosan coated sample was higher than that of uncoated sample. This was similar to the obtained results of electrophoretic deposition of chitosan on mild steel alloy [38].

Table 1 compares the simulated results of the experimental data of the samples using electrical circuits. The chitosan coating on the surface of stainless steel increased the total resistance (total resistance of the inner and outer layer) and reduced the CPE_{ox} of the native oxide layer of stainless steel, similar to reported results for chitosan coating on NiTi alloy [36]. Moreover, the addition of Cu nanoparticles increased the total resistance of the coatings that could be due to the formation of Cu oxide layer on the surface. Generally, the total resistance of the coatings was enhanced by increasing the Cu concentration up to 0.5 wt%, and reduced for higher Cu concentration.

The Tafel polarization curves of the samples, after immersion in SBF (pH = 7.4) at room temperature, are presented in Fig. 10. The cathodic and anodic branches of the polarization curves represent the release of hydrogen gas and the dissolution of the coating and substrate, respectively. The corrosion potential values (E_{corr}) of Ch-0.25Cu and Ch-0.5Cu samples were remarkably higher than those of the uncoated and chitosan coated sample. The presence of Cu nanoparticles reduced the tendency of the coating to corrode due to the nobility of Cu. The corrosion current density value (i_{corr}) of the chitosan coated sample was significantly lower than that of the uncoated sample. This result is in a good agreement with the reported results in Ref [23]. Moreover, the i_{corr} values of all chitosan-copper nanocomposite coated samples were lower than the i_{corr} value of the chitosan coated sample except for the coated sample containing 1.25% Cu nanoparticles. Although the E_{corr} value of the Ch-1Cu sample was lower than that of the chitosan coated sample, which could be due to the agglomeration of Cu nanoparticles, its i_{corr} value was much lower than i_{corr} value of the chitosan coated sample. This represented that the corrosion resistance of Ch-1Cu coating was higher than that of the chitosan coated sample. The both E_{corr} and i_{corr} values of the Ch-1.25Cu sample were lower than those of the chitosan coated sample. It could be probably due to the low bonding adhesion of the coating/substrate. On the other hand, by increasing the

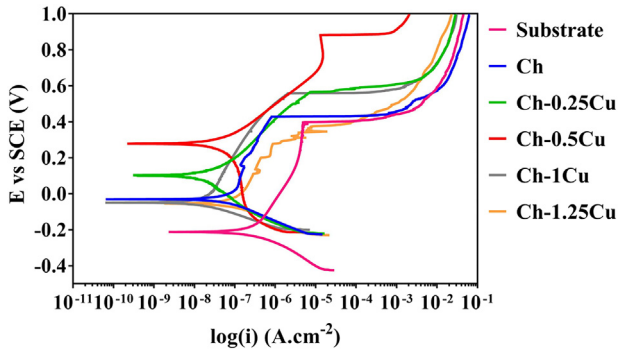

Fig. 10. Electrochemical Tafel polarization curves of samples after immersion in SBF (pH = 7.4) at room temperature.

Table 2
Extracted values of electrochemical parameters of Tafel polarization curves.

Coating types	Ecorr (mV)	icorr ($\mu A/cm^2$)	βa (mV/dec)	-βc (mV/dec)	Eb (mV)
Substrate	−214.522	158.072	0.128	0.007	399.337
Ch	−30.258	88.696	1.406	0.037	428.512
Ch-0.25Cu	103.565	57.712	0.195	0.098	566.538
Ch-0.5Cu	278.316	20.375	0.068	0.556	884.275
Ch-1Cu	−55.687	38.801	1.947	0.472	561.101
Ch-1.25Cu	−57.242	92.066	0.210	0.035	380.608

Cu concentration up to 0.5 wt%, the corrosion resistance of the coatings increased. However, with higher Cu concentration, the corrosion resistance of coatings reduced. The electrochemical polarization results are in a good agreement with the electrochemical impedance results.

Table 2 shows the extracted values of the electrochemical parameters from the Tafel polarization curves. The break down potential value (E_b) of the chitosan sample was higher than that of the uncoated sample, which indicated an increase in the local corrosion resistance of the stainless steel. In addition, the E_b values of all chitosan-copper nanocomposite coated samples were higher than the E_b value of the chitosan coated sample except for the highest Cu concentration. This could indicate an improvement in the local corrosion resistance of the coatings by including Cu nanoparticles in the chitosan matrix. By increasing the Cu concentration from 0.25 to 0.5 wt%, the E_b values reached from 566.538 to 884.275. While they were reduced with Cu concentration higher than 0.5 wt%. The slope of the extrapolated cathodic branch ($-\beta c$) of the chitosan coated sample was higher than that of the uncoated substrate. The same results were reported for chitosan coating on Mg−1Ca alloy [7], indicating an increase in the rate of hydrogen gas release and the corrosion resistance of the coating. Moreover, by increasing the Cu concentration up to 0.5 wt%, the slope of the cathodic branch firstly increased and then declined, which could be due to the formation of pores in the coating.

The polarization resistance (Rp) of the samples was calculated according to the following relation (Eq. (3)):

$$Rp = (\beta c \times \beta a)/(2.303 \times i_{corr} \times (\beta c + \beta a)) \quad (3)$$

where βa and βc are the slope of the extrapolated anodic and cathodic branches, respectively (Table 2). Moreover, the protective efficiency (PE) was calculated according to the following relation (Eq. (4)):

$$PE = (1 - i_{corr}/i_0) \times 100 \quad (4)$$

where i_0 and i_{corr} are the corrosion density of the uncoated and coated samples, respectively (Table 2). The results are shown in Fig. 11. The presence of chitosan coating on the stainless steel surface caused an increase in the Rp value. The PE value of chitosan coated sample on stainless steel (43%) was lower than reported data for the chitosan coated on NiTi alloy (97.7%) in ref. [36]. The reason for this was the lower corrosion rate of stainless steel compared to NiTi alloy, which led less protective efficiency of chitosan coatings. Furthermore, including of Cu nanoparticles up to 0.5% increased both R_p and PE values and

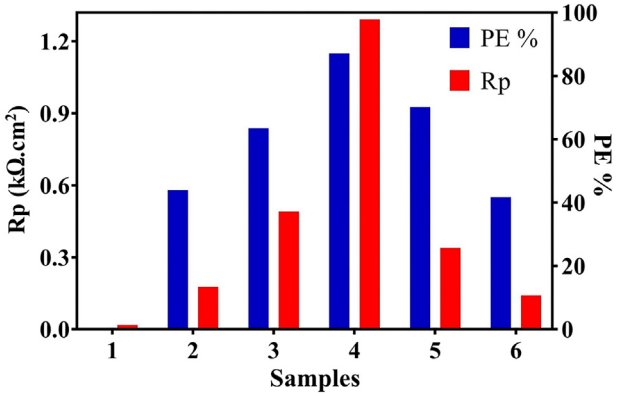

Fig. 11. Polarization resistance and protective efficiency of 1) blank substrate 2) Ch 3) Ch-0.25Cu 4) Ch-0.5Cu 5) Ch-1Cu 6) Ch-1.25Cu.

Table 3
Antibacterial activity of samples. (Log (bacteria concentration)).

Samples	Control	Steel	Ch	Ch-0.25Cu	Ch-0.5Cu	Ch-1Cu	Ch-1.25Cu
E. coli	6	5.57	3.94	2.52	2.4	2.06	2
S. aureus	6	5.64	4.17	0	0	0	0

therefore enhanced the corrosion resistance of the coating. The corrosion resistance of chitosan-Cu nanocomposite samples was influenced by the Cu concentration. Increasing the Cu concentration up to 0.5 wt% caused an increase in the R_p and PE values. However, there was a decrease in the R_p and PE values for higher Cu concentrations. The PE value of the Ch-0.5Cu sample (87%) was lower than chitosan coating containing gold nanoparticles on NiTi alloy (99.2%) [36]. This might be because the corrosion rate of stainless steel was lower than NiTi alloy, as well as because the corrosion resistance of Au nanoparticles was higher than that of Cu nanoparticles.

3.4. Antibacterial activity of the nanocomposite coatings

Cu nanoparticles, as metal nanoparticles, must release Cu ions to kill the bacteria, hence the steady and continuous release of Cu ions are the crucial feature in the fabrication of an antibacterial coating containing Cu nanoparticles [39,40]. The agglomeration of Cu nanoparticles significantly affects the antibacterial activity of the coating by reducing the ions release, in fact, particles consisted of high specific surface area show the higher release of ions release [39]. Due to the fact that the antibacterial activity of Cu nanoparticles relies on the release of Cu ions, the insertion of the Cu nanoparticles into an organic polymer matrix, such as chitosan, is one of the most effective methods to increase the release of Cu ions, since organic polymer matrix acts as a suitable medium to stabilize and avoid the aggregation of the Cu nanoparticles [40]. According to the literature, it has been reported that chitosan and copper have partial antimicrobial activity against both Gram-negative and Gram-positive bacteria [8,15]. Therefore, compared to individual copper or chitosan, the antibacterial activity of chitosan-copper nanocomposite coating should be significantly higher than individual chitosan coating.

Table 3 shows the antibacterial behavior of different coatings against Gram-positive (*S. aureus*) and Gram-negative (*E. coli*) bacteria in comparison to the reference sample (316L stainless steel substrate). It is obvious that 316L stainless steel did not show antibacterial activity and a number of bacteria remained intact. As soon as chitosan coating was deposited on the substrate, antibacterial activity embarked to gradually increase, and most interestingly, as copper nanoparticles were added into a polymeric matrix, the antibacterial activity of chitosan-copper nanocomposite coating was dramatically improved against both types of bacteria. The best results against both types of bacteria were related to the Cu concentration > 0.5 wt%. However, the addition of a higher amount of copper (over 1% of copper nanoparticles) made an insignificant change in the antibacterial activity of complex and this trend stayed constant. It could be due to the agglomeration of Cu nanoparticles in the chitosan matrix. Nanocomposite coatings exhibited an almost similar trend against both types of bacteria. The obtained results were in good agreement with the reported results for antibacterial activities of Cu nanoparticle doped chitosan studied by Wen-Li et al. [18].

4. Conclusions

In the current research, electrophoretic deposition was successfully applied for in-situ deposition of antibacterial and anticorrosion chitosan-copper nanocomposite coating on stainless steel substrates by in situ electrophoretic method. It was concluded that using a chemical method and the presence of chitosan as stabilizer could be a suitable procedure to achieve copper nanoparticles with particle size around 11 nm. The nanocomposite coating exhibited high quality surface and acceptable adhesion in comparison to a pure chitosan coating. An optimum condition resulted from controlled the deposition of chitosan and copper nanoparticles was related to the suspension with Cu concentration of 0.5%.

The presence of chitosan coating on the stainless steel surface, especially the addition of Cu nanoparticles, increased the corrosion resistance of the substrate. Corrosion resistance of chitosan-copper nanocomposite coated samples was influenced by the Cu concentration and the agglomeration of nanoparticles. Thus, the Ch-0.5Cu sample had the highest corrosion resistance.

Results obtained from the antibacterial activity tests on nanocomposite coatings showed that the chitosan-copper coating exhibited more deadly influence on both positive and negative charge bacteria. Although there was no significant difference in the antibacterial activity of Ch-1Cu and Ch-1.25Cu samples, the most successful result of an antibacterial test against gram-negative and gram-positive bacteria were attributed to sample containing 1.25 wt% of copper nanoparticles.

References

[1] J. Song, Q. Chen, Y. Zhang, M. Diba, E. Kolwijck, J. Shao, J.A. Jansen, F. Yang, A.R. Boccaccini, S.C. Leeuwenburgh, Electrophoretic deposition of chitosan coatings modified with gelatin nanospheres to tune the release of antibiotics, ACS Appl. Mater. Interfaces 8 (2016) 13785–13792.
[2] Q. Chen, W. Li, O.-M. Goudouri, Y. Ding, S. Cabanas-Polo, A.R. Boccaccini, Electrophoretic deposition of antibiotic loaded PHBV microsphere-alginate composite coating with controlled delivery potential, Colloids Surf. B: Biointerfaces 130 (2015) 199–206.
[3] C.K. Seal, K. Vince, M. Hodgson, Biodegradable surgical implants based on magnesium alloys—a review of current research, IOP Conference Series: Materials Science and Engineering, IOP Publishing, 2009, p. 012011.
[4] S.B. Goodman, Z. Yao, M. Keeney, F. Yang, The future of biologic coatings for orthopaedic implants, Biomaterials 34 (2013) 3174–3183.
[5] D. Campoccia, L. Montanaro, C.R. Arciola, A review of the clinical implications of anti-infective biomaterials and infection-resistant surfaces, Biomaterials 34 (2013) 8018–8029.
[6] J. Hu, C. Zhang, B. Cui, K. Bai, S. Guan, L. Wang, S. Zhu, In vitro degradation of AZ31 magnesium alloy coated with nano TiO_2 film by sol–gel method, Appl. Surf. Sci. 257 (2011) 8772–8777.
[7] X. Gu, Y. Zheng, Q. Lan, Y. Cheng, Z. Zhang, T. Xi, D. Zhang, Surface modification of an Mg-1Ca alloy to slow down its biocorrosion by chitosan, Biomed. Mater. 4 (2009) 044109.
[8] H. Mokhtari, Z. Ghasemi, M. Kharaziha, F. Karimzadeh, F. Alihosseini, Chitosan-58S bioactive glass nanocomposite coatings on TiO_2 nanotube: structural and biological properties, Appl. Surf. Sci. 441 (2018) 138–149.
[9] W. Chen, Y. Liu, H. Courtney, M. Bettenga, C. Agrawal, J. Bumgardner, J. Ong, In vitro anti-bacterial and biological properties of magnetron co-sputtered silver-containing hydroxyapatite coating, Biomaterials 27 (2006) 5512–5517.
[10] K. Bai, Y. Zhang, Z. Fu, C. Zhang, X. Cui, E. Meng, S. Guan, J. Hu, Fabrication of chitosan/magnesium phosphate composite coating and the in vitro degradation properties of coated magnesium alloy, Mater. Lett. 73 (2012) 59–61.
[11] G.R. Saad, M.A. Elsawy, M.Z. Elsabee, Preparation, characterization and antimicrobial activity of poly (3-hydroxybutyrate-co-3-hydroxyvalerate)-g-poly (*N*-vinylpyrrolidone) copolymers, Polym.-Plast. Technol. Eng. 51 (2012) 1113–1121.
[12] X. Pang, T. Casagrande, I. Zhitomirsky, Electrophoretic deposition of

hydroxyapatite–$CaSiO_3$–chitosan composite coatings, J. Colloid Interface Sci. 330 (2009) 323–329.
[13] X. Pang, I. Zhitomirsky, Electrophoretic deposition of composite hydroxyapatite-chitosan coatings, Mater. Charact. 58 (2007) 339–348.
[14] E. Alzahrani, R.A. Ahmed, Synthesis of copper nanoparticles with various sizes and shapes: application as a superior non-enzymatic sensor and antibacterial agent, Int. J. Electrochem. Sci. 11 (2016) 4712–4723.
[15] J. Ramyadevi, K. Jeyasubramanian, A. Marikani, G. Rajakumar, A.A. Rahuman, Synthesis and antimicrobial activity of copper nanoparticles, Mater. Lett. 71 (2012) 114–116.
[16] M. Guzman, J. Dille, S. Godet, Synthesis and antibacterial activity of silver nanoparticles against gram-positive and gram-negative bacteria, Nanomedicine 8 (2012) 37–45.
[17] V.K. Sharma, R.A. Yngard, Y. Lin, Silver nanoparticles: green synthesis and their antimicrobial activities, Adv. Colloid Interf. Sci. 145 (2009) 83–96.
[18] W.-L. Du, S.-S. Niu, Y.-L. Xu, Z.-R. Xu, C.-L. Fan, Antibacterial activity of chitosan tripolyphosphate nanoparticles loaded with various metal ions, Carbohydr. Polym. 75 (2009) 385–389.
[19] S.-H. Jun, E.-J. Lee, S.-W. Yook, H.-E. Kim, H.-W. Kim, Y.-H. Koh, A bioactive coating of a silica xerogel/chitosan hybrid on titanium by a room temperature sol–gel process, Acta Biomater. 6 (2010) 302–307.
[20] T. da S. Pinto, L.A. Alves, G. de Azevedo Cardozo, V.H.O. Munhoz, R.M. Verly, F.V. Pereira, J.P. de Mesquita, Layer-by-layer self-assembly for carbon dots/chitosan-based multilayer: morphology, thickness and molecular interactions, Mater. Chem. Phys. 186 (2017) 81–89.
[21] F. Sun, X. Pang, I. Zhitomirsky, Electrophoretic deposition of composite hydroxyapatite–chitosan–heparin coatings, J. Mater. Process. Technol. 209 (2009) 1597–1606.
[22] A. Boccaccini, S. Keim, R. Ma, Y. Li, I. Zhitomirsky, Electrophoretic deposition of biomaterials, J. R. Soc. Interface 7 (2010) S581–S613.
[23] F. Gebhardt, S. Seuss, M. Turhan, H. Hornberger, S. Virtanen, A.R. Boccaccini, Characterization of electrophoretic chitosan coatings on stainless steel, Mater. Lett. 66 (2012) 302–304.
[24] L. Besra, M. Liu, A review on fundamentals and applications of electrophoretic deposition (EPD), Prog. Mater. Sci. 52 (2007) 1–61.
[25] Y. Li, K. Wu, I. Zhitomirsky, Electrodeposition of composite zinc oxide–chitosan films, Colloids Surf. A Physicochem. Eng. Asp. 356 (2010) 63–70.
[26] F. Ashrafizadeh, Adhesion evaluation of PVD coatings to aluminium substrate, Surf. Coat. Technol. 130 (2000) 186–194.
[27] T. Kokubo, H. Takadama, How useful is SBF in predicting in vivo bone bioactivity? Biomaterials 27 (2006) 2907–2915.
[28] M.S. Usman, N.A. Ibrahim, K. Shameli, N. Zainuddin, W.M.Z.W. Yunus, Copper nanoparticles mediated by chitosan: synthesis and characterization via chemical methods, Molecules 17 (2012) 14928–14936.
[29] M.S. Usman, M.E. El Zowalaty, K. Shameli, N. Zainuddin, M. Salama, N.A. Ibrahim, Synthesis, characterization, and antimicrobial properties of copper nanoparticles, Int. J. Nanomedicine 8 (2013) 4467.
[30] O.A. Monteiro Jr., C. Airoldi, Some thermodynamic data on copper–chitin and copper–chitosan biopolymer interactions, J. Colloid Interface Sci. 212 (1999) 212–219.
[31] F. Brunel, N.E. El Gueddari, B.M. Moerschbacher, Complexation of copper (II) with chitosan nanogels: toward control of microbial growth, Carbohydr. Polym. 92 (2013) 1348–1356.
[32] T.M.D. Dang, T.T.T. Le, E. Fribourg-Blanc, M.C. Dang, Synthesis and optical properties of copper nanoparticles prepared by a chemical reduction method, Adv. Nat. Sci. Nanosci. Nanotechnol. 2 (2011) 015009.
[33] I. Zhitomirsky, L. Gal-Or, Electrophoretic deposition of hydroxyapatite, J. Mater. Sci. Mater. Med. 8 (1997) 213–219.
[34] A. Simchi, F. Pishbin, A. Boccaccini, Electrophoretic deposition of chitosan, Mater. Lett. 63 (2009) 2253–2256.
[35] K. Grandfield, I. Zhitomirsky, Electrophoretic deposition of composite hydroxyapatite–silica–chitosan coatings, Mater. Charact. 59 (2008) 61–67.
[36] R.A. Ahmed, S.A. Fadl-allah, N. El-Bagoury, S.M.G. El-Rab, Improvement of corrosion resistance and antibacterial effect of NiTi orthopedic materials by chitosan and gold nanoparticles, Appl. Surf. Sci. 292 (2014) 390–399.
[37] G. Brug, A. Van Den Eeden, M. Sluyters-Rehbach, J. Sluyters, The analysis of electrode impedances complicated by the presence of a constant phase element, J. Electroanal. Chem. Interfacial Electrochem. 176 (1984) 275–295.
[38] R.A. Ahmed, R. Farghali, A. Fekry, Study for the stability and corrosion inhibition of electrophoretic deposited chitosan on mild steel alloy in acidic medium, Int. J. Electrochem. Sci. 7 (2012) 7270–7282.
[39] R. Kumar, H. Münstedt, Silver ion release from antimicrobial polyamide/silver composites, Biomaterials 26 (2005) 2081–2088.
[40] R. Rawashdeh, Y. Haik, Antibacterial mechanisms of metallic nanoparticles: a review, Dyn. Biochem. Process. Biotechnol. Mol. Biol. 3 (2009) 12–20.